Acta Pharmaceutica Sinica B 2022;12(2):924–938

Chinese Pharmaceutical Association
Institute of Materia Medica, Chinese Academy of Medical Sciences

Acta Pharmaceutica Sinica B

www.elsevier.com/locate/apsb
www.sciencedirect.com

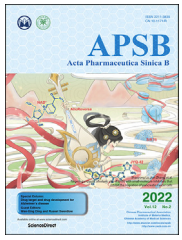

ORIGINAL ARTICLE

Enhanced tumor homing of pathogen-mimicking liposomes driven by R848 stimulation: A new platform for synergistic oncology therapy

Xiaobei Cheng[a,†], Pei Yu[a,†], Xiang Zhou[b], Jiale Zhu[a], Yubao Han[a], Chao Zhang[a,*], Lingyi Kong[a,*]

[a]*State Key Laboratory of Natural Medicines, Jiangsu Key Laboratory of Bioactive Natural Product Research, School of Traditional Chinese Pharmacy, China Pharmaceutical University, Nanjing 210009, China*
[b]*Department of Science, China Pharmaceutical University, Nanjing 210009, China*

Received 9 April 2021; received in revised form 20 June 2021; accepted 2 July 2021

KEY WORDS

Resiquimod;
Neutrophil infiltration;
Liposomes;
Drug delivery;
Pathogen-mediated tumor targeting;
Combination therapy;
Nano therapy;
Chemotherapy

Abstract Although multifarious tumor-targeting modifications of nanoparticulate systems have been attempted in joint efforts by our predecessors, it remains challenging for nanomedicine to traverse physiological barriers involving blood vessels, tissues, and cell barriers to thereafter demonstrate excellent antitumor effects. To further overcome these inherent obstacles, we designed and prepared mycoplasma membrane (MM)-fused liposomes (LPs) with the goal of employing circulating neutrophils with the advantage of inflammatory cytokine-guided autonomous tumor localization to transport nanoparticles. We also utilized *in vivo* neutrophil activation induced by the liposomal form of the immune activator resiquimod (LPs-R848). Fused LPs preparations retained mycoplasma pathogen characteristics and achieved rapid recognition and endocytosis by activated neutrophils stimulated by LPs-R848. The enhanced neutrophil infiltration in homing of the inflammatory tumor microenvironment allowed more nanoparticles to be delivered into solid tumors. Facilitated by the formation of neutrophil extracellular traps (NETs), podophyllotoxin (POD)-loaded MM-fused LPs (MM-LPs-POD) were concomitantly released from neutrophils and subsequently engulfed by tumor cells during inflammation. MM-LPs-POD displayed superior suppression efficacy of tumor growth and lung metastasis in a 4T1 breast tumor model. Overall, such a strategy of pathogen-mimicking nanoparticles hijacking neutrophils *in situ* combined with enhanced neutrophil infiltration indeed elevates the potential of chemotherapeutics for tumor targeting therapy.

*Corresponding author. Tel./fax: +86 25 83271405.
E-mail addresses: zhangchao@cpu.edu.cn (Chao Zhang), cpu_lykong@126.com (Lingyi Kong).
[†]These authors made equal contributions to this work.
Peer review under responsibility of Chinese Pharmaceutical Association and Institute of Materia Medica, Chinese Academy of Medical Sciences.

https://doi.org/10.1016/j.apsb.2021.08.018

1. Introduction

Accounting for 10%−20% of breast cancer cases, triple-negative breast cancer (TNBC) with high metastasis, recurrence and mortality rates has always been a serious life threat for young women[1]. Over the past few decades, nanomedicine has achieved great progress in the field of tumor-targeted drug delivery[2−5]. Nevertheless, due to the clearance of the reticuloendothelial system (RES), the aberrant and complex tumor vascular structure, the dense extracellular matrix, and the elevated interstitial fluid pressure, nanoparticles have not accumulated in tumors as expected despite various tumor active targeting modifications[6].

Serving as the most abundant leukocytes in peripheral blood, neutrophils are the front-line killer cells in innate immunity[7]. In addition to the tumor-killing effect of drugs released through the self-apoptosis and the formation of neutrophil extracellular traps (NETs) in the presence of inflammatory signal, neutrophils themselves could also inhibit tumor growth. On the one hand, once neutrophils are in direct contact with the tumor cells, the secretion of reactive oxygen species (ROS) through the respiratory burst comes into play[8]. On the other hand, neutrophils could act by activating dendritic cells, $CD4^+$ and $CD8^+$ cells[9]. Neutrophils have a strong ability to move across the blood vessels through a special molecular mechanism and can also migrate to the inflammatory tumor site under chemotaxis, and even penetrate the deep avascular regions of tumors[10]. Consequently, the strategy of transportation by neutrophils based on their inflammation localization abilities has been proposed as an emerging concept for enhanced nanodrug delivery[11−13]. The first step of utilizing neutrophils for drug delivery is to assemble neutrophil-nanoparticle complexes, which can be completed in two approaches. One approach is to co-incubate neutrophils with nanoparticles *in vitro* to accomplish the loading of nanoparticles[12], followed by transfusion back into bodies. In the other strategy, nanoparticles are able to hijack neutrophils *in situ*[14]. However, the method of extracorporeal loading still involves some challenges, including the terminal differentiation of neutrophils with a short lifetime (~7 h) and the lack of a mature and stable culture method *ex vivo*. In addition, it can be dangerous to inject a large number of cells at once because of systemic toxicity, and external contamination may also occur occasionally. The latter approach could be convenient in clinical practice, but the solution lies in the design of nanoparticles[15]. The rational design of delivery systems to target neutrophils *in vivo* has been utilized in studies to achieve increased nanoparticle deposition in tumor sites[16,17].

Neutrophils recognize and swallow foreign invaders through pathogen-associated molecular patterns (PAMPs) by Toll-like receptors[18]. Hybrid integration of bacteria-derived outer membrane vesicles (OMVs), defined as a potential nanoplatform, has been reported to improve tumor immunity and photothermal treatment efficiency[19−21]. However, the shortcomings of low yields and cumbersome extraction methods have limited their development in the field of drug delivery to a certain extent. Herein, we constructed a drug delivery system utilizing the mycoplasma membrane (MM) as a substitute, which has the characteristics of large productivity and easy availability benefits from the absence of a cell wall[22], followed by fusion with drug-loading liposomes (LPs) to enhance their pathogen properties, thus promoting neutrophil uptake. Furthermore, a dual Toll-like receptor 7/8 (TLR7/8) agonist R848 was added to recruit more neutrophils into the tumor region because of the ability to induce acute inflammation[23,24]. Although R848 has been widely reported as an antitumor immunomodulator[25−29], studies leveraging its effects on neutrophils to aid nanodrug delivery are lacking. Accordingly, our design can simultaneously improve the phagocytosis of MM decorated LPs by activated neutrophils[30,31], and enhance nanodrug accumulation along with the homing of neutrophils[19]. To minimize unwanted immune side effects, we encapsulated R848 in LPs (LPs-R848) to control the action site of the blood and tumor. This joint strategy aimed to promote the most beneficial outcome, which both replenished the insufficient antitumor efficacy of R848 itself[28] and accelerated the delivery of nanoparticles deep into tumors. In practice, the injection of LPs-R848 was anterior to the drug-loaded nanoparticles to pre-create an inflammatory environment. The use of podophyllotoxin (POD), an outstanding antitumor chemotherapeutic drug, is limited due to the fatal drawback of systemic toxicity, especially unacceptable gastrointestinal toxicity[32,33]. Our delivery system coupled with POD (MM-LPs-POD) was confirmed to notably inhibit tumor growth and lung metastasis in a 4T1 breast cancer model (Scheme 1). In summary, we envision that the combination of nanomedicine based on cell delivery and clinical therapy could provide a realizable means for tumor targeted treatment.

2. Materials and methods

2.1. Materials

Soya bean lecithin (SPC) and cholesterol (Chol) were purchased from Sangon Biotech (Shanghai, China). Podophyllotoxin (POD) and resiquimod (R848) were provided by CSNpharm (Chicago, IL, USA). Percoll, collagenase IV, DNase I, D-luciferin, HRP-conjugated secondary antibody and fluorescence dyes, including DiD, DiI, and DiO, were supplied by Shanghai Yeason Bio Technologies Co., Ltd. (Shanghai, China). ACK lysis buffer was purchased from Beyotime Institute of Biotechnology (Nantong, China). All antibodies used for flow cytometry were purchased from Biolegend (San Diego, CA, USA). Anti-P97 antibody was purchased from Genscript (Nanjing, China). Anti-Ly6G antibody for IHC and Cy3 conjugated anti-MPO antibody for IF were purchased from abcam (Shanghai, China). The other chemicals and reagents were all analytical grade.

2.2. Cell lines and mice

4T1 breast cancer cells were obtained from Shanghai Cell Bank, Chinese Academy of Sciences (CAS, Shanghai, China). 4T1 cells with stable luciferase expression (4T1-luc cells) were established through lentiviral transfection (Hanbio, Shanghai, China). Both cell lines were cultured in RPMI 1640 containing 10% FBS and

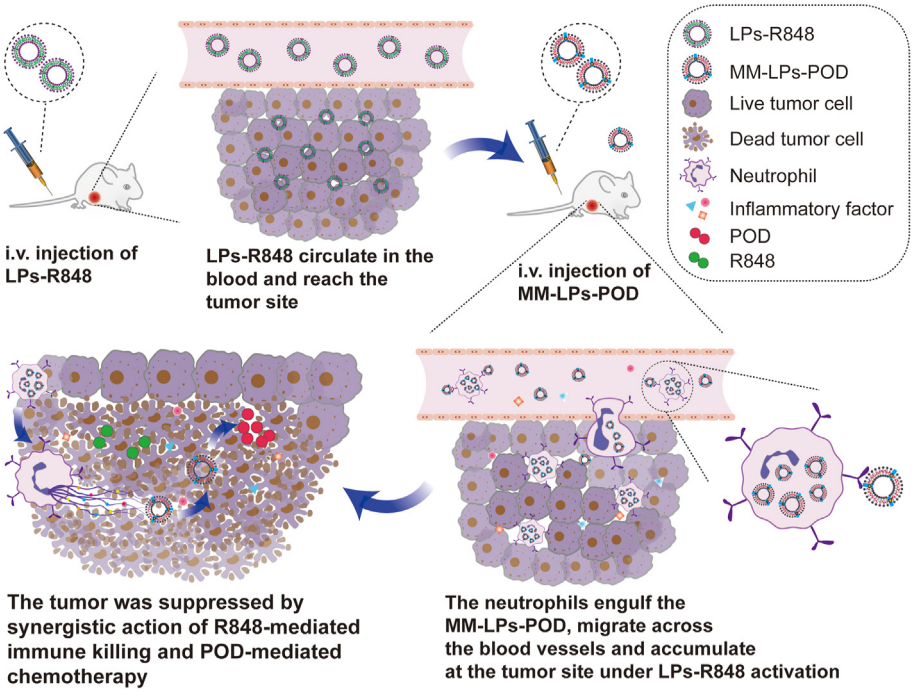

Scheme 1 Schematic illustration of the combination of LPs-R848 with MM-LPs-POD for synergistic tumor therapy.

1% nonessential amino acids. Cells were kept in 5% CO_2 and 37 °C with a humidified atmosphere.

Female BALB/c mice (aged 7−8 weeks) and Sprague−Dawley (SD) rats (180−220 g) were provided by Shanghai Laboratory Animal Research Center (Shanghai, China). Prior to the experiment, mice were acclimatized for 5 days in a specific pathogen-free facility with human care. All animal experiments were in compliance with the animal care regulations of China Pharmaceutical University.

2.3. *Preparation and characterization of MM-LPs-POD*

POD-loaded LPs (LPs-POD) were prepared by a thin-film hydration method. In general, 30 mg of SPC, 3 mg of Chol, and 2 mg of POD were dissolved in methanol and chloroform (2:1, *v*/*v*), and then the solvent was evaporated in a round flask to form a thin film, which was subsequently hydrated with double-distilled water and sonicated at 4 °C for 5 min to make a uniform LPs solution. LPs-POD were then centrifuged at 3000 rpm (ST16R, ThermoFisher Scientific, Waltham, MA, USA) for 10 min and microfiltered through a filter membrane (0.22 μm) to remove free POD. To prepare MM-LPs-POD, different proportions of MM (lipid:overall protein ratios of 2:0.04, 2:0.2, and 2:0.1, by weight) were added to LPs-POD and stirred at 37 °C for 1 h followed by extrusion through 0.1 μm polycarbonate membranes (Avanti Polar Lipids, Alabaster, AL, USA) 11 times at room temperature. MM-LPs-POD were stored at 4 °C until use. The preparation methods of LPs-R848, DiD-loaded LPs (LPs-DiD), DiD-loaded MM-LPs (MM-LPs-DiD) and DiO-loaded MM-LPs (MM-LPs-DiO) were all similar. MM-derived nanovesicles (MMVs) were prepared by direct extrusion.

The size distribution, zeta potential, and polydispersity index (PDI) were measured by dynamic light scattering (DLS, Zetasizer 3000HS, Malvern Panalytical, Shanghai, China). The diameters of nanoparticles in saline or with 10% serum at 37 °C and 4 °C were detected at different time points to investigate stability. The morphology and structure of the nanoparticles were evaluated by transmission electron microscopy (TEM, HT7700, HITACHI, Tokyo, Japan) through phosphotungstic acid staining. The protein components of MM-LPs were analyzed by SDS-PAGE assay. Briefly, all samples were normalized to equal protein concentrations *via* the BCA method and prepared in loading buffer (Bio-Rad, Hercules, CA, USA). Samples were loaded onto a 10% SDS-polyacrylamide gel and followed by silver staining. The typical cell membrane protein (P97) on MMVs and MM-LPs was examined by western blotting assay. All the samples were prepared and loaded onto a 10% SDS-polyacrylamide gel for protein separation as described above. The proteins were next transferred polyvinylidene difluoride membranes (Millipore, Billerica, MA, USA) and probed with anti-P97 antibody, followed by staining with HRP-conjugated secondary antibody. Proteins were finally detected using Bio-Rad ChemiDoc XRS+.

2.4. *Membrane fusion verification*

Förster resonance energy transfer (FRET) was used to estimate the fusion of MM and LPs. DiI and DiD were encapsulated in LPs by the same method mentioned above. MM was added to LPs in varying proportions, stirred, and extruded to facilitate membrane fusion. The fluorescence spectrum of the final double-dyed nanoparticles was detected from 550 to 725 nm by a SpectraMax Paradigm Multimode Detection Platform (Molecular Devices, Sunnyvale, CA, USA) using 550 nm as the excitation wavelength.

2.5. *In vitro release profiles of LPs-POD and MM-LPs-POD*

The *in vitro* drug release behaviors of LPs-POD and MM-LPs-POD were determined by the dialysis method in PBS at different pH values of 7.4 and 4.5. In brief, 3 mL of the two

freshly prepared POD preparations were sealed in dialysis bags (MWCO 3500) and then immersed in 50 mL of release medium (containing 0.1% Tween 80). Then, the cells were incubated in a constant temperature shaker with gentle agitation. The released solution (0.5 mL) was collected and replaced with fresh medium at predetermined time intervals. The POD concentrations were determined using high-performance liquid chromatography (HPLC, Agilent 1290 Infinity, Agilent, CA, USA).

2.6. *Effect of LPs-R848 on neoplastic infiltration of neutrophils*

For dose exploration of R848, tumor-bearing mice were i.v. injected with LPs-R848 when the tumor volume reached 200 mm^3 at doses of 1, 5, 10, and 20 μg per mouse. At predetermined time points, peripheral blood and tumors were collected, and the ratios of neutrophils in $CD45^+$ cells were analyzed by flow cytometry (Accuri C6, BD, Franklin Lakes, NJ, USA). The data obtained were analyzed by FlowJo V10 software (BD).

For blood samples, after 5 min of erythrocyte lysis, cells were rinsed with PBS three times and incubated with APC-CD45, FITC-CD11b, and PE/Cy7-Ly6G antibodies for 15 min. The samples were centrifuged at 350×*g* for 5 min and washed three times before testing. For tumor tissues, after excision from the living mice, tumors were rapidly incubated in a digestive solution consisting of 0.1% collagenase IV and 0.02% DNase I for 30 min with gentle shaking to prepare a single-cell suspension. Afterward, the cell suspension was filtered through a cell strainer and centrifuged at 350×*g* for 5 min to sediment the cells. After erythrocyte lysis, cells were blocked with CD16/32 for 15 min to exclude nonspecific binding, followed by staining with the three fluorescent antibodies mentioned above, washing with PBS, and finally analyzing by flow cytometry (BD).

2.7. *In vivo ingestion of nanoparticles by neutrophils*

It was determined whether LPs-POD and MM-LPs-POD could hijack circulating neutrophils in the blood, thus targeting and accumulating in tumor sites. Flow cytometry (BD) was used to analyze the ratios of neutrophils containing nanoparticles to total $CD11b^+$ and $Ly6G^+$ neutrophils in blood samples and tumor tissues. Briefly, tumor-bearing mice were i.v. injected or not with LPs-R848 at a dose of 5 μg per mouse in advance. One hour later, LPs-DiD or MM-LPs-DiD were i.v. injected into untreated or LPs-R848-treated mice. Samples of peripheral blood and tumors were collected at predetermined time intervals and processed using the same methods described above except staining only with FITC-CD11b and PE/Cy7-Ly6G antibodies, and the samples were then tested by flow cytometry (BD). The data obtained were analyzed by FlowJo V10 software (BD).

2.8. *In vivo live imaging*

A MaestroTM *in vivo* imaging system (PerkinElmer, Waltham, MA, USA) was applied to investigate the distribution and tumor-targeting ability of nanoparticles. LPs-DiD and MM-LPs-DiD with different proportions of MM were i.v. injected into mice, and images were taken at predetermined time intervals. For the combination group, LPs-R848 were i.v. injected 1 h before injecting nanoparticles. At 48 h post injection, the mice were sacrificed, and tumors and main organs were dissected for *ex vivo* imaging to display the organ distribution of the nanoparticles. Living Image Software (PerkinElmer) was used for data analysis.

2.9. *Real-time qPCR*

Tumor-bearing mice were i.v. injected or not with LPs-R848 at a dose of 5 μg per mouse. Four hours later, a tissue RNA extraction kit (ESscience, Shanghai, China) was used to extract total RNA from organs, including the liver, spleen, and tumor, according to the manufacturer's instructions. The RNA was reverse transcribed to cDNA using a reverse transcription kit (Vazyme, Nanjing, China). Quantitative real-time PCR (qPCR) analyses were conducted using SYBR Green Master Mix (Vazyme) and a LightCycler 480 Detector (Roche, Mannheim, Germany)[34]. The primers used are provided in the (Supplementary Materials Table 1). The results were calculated through the comparative $2^{-\triangle\triangle Ct}$ method with *Gaphd* as an endogenous control.

2.10. *Isolation of mature neutrophils from mouse bone marrow*

Mature neutrophils were isolated from bone marrow through the commonly used density gradient centrifugation method. Briefly, bones detached from mouse legs were immersed in RPMI 1640 medium, and then both ends of the bone were cut to expose the marrow cavity. The cells inside were flushed out with PBS, filtered through a cell strainer and centrifuged at 350 *g* for 5 min to collect bone marrow cells. After depleting red blood cells for 10 min on ice, the cells were washed with PBS three times. Afterward, the cell suspension was added to the top layer of separation solution containing 55%, 65% and 75% Percoll mixture solution, followed by centrifugation at 800 *g* for 40 min at room temperature. Neutrophils were collected at the interface of 65% and 75% fractions and washed three times with ice-cold PBS. The viability of the obtained neutrophils was detected by trypan blue staining, while the purity was analyzed using flow cytometry (BD) by double staining with FITC-CD11b and PE/Cy7-Ly6G antibodies.

2.11. *Evaluation of physiological activities of neutrophils under inflammation*

The physiological functions of neutrophils isolated from mice were evaluated, including the expression of the specific adhesion molecules CD11b and CD44. Neutrophils were incubated in culture medium with or without formylmethionylleucylphenylalanine (fMLP) at concentrations of 0, 10, and 100 nmol/L for 30 min. Thereafter, the cells were washed three times with PBS and stained with FITC-CD11b or APC-CD44 antibodies. Finally, flow cytometry (BD) was used to determine the fluorescence signal. To evaluate the *in vivo* tumor infiltration ability of neutrophils before and after administration of nanoparticles, 4T1-bearing mice were treated with LPs-R848 in advance. After 1 h, PBS and different nanoparticles were i.v. injected into mice. Four hours later, tumors were excised, and the ratios of neutrophils to tumor cells were analyzed by flow cytometry (BD).

2.12. *Formation of NETs in vitro and in vivo*

For *in vitro* experiment, the isolated neutrophils (1×10^4 cells) were seeded in a 96-well plate and incubated with or without 100 nmol/L PMA for 8 h. After washing slightly with PBS thrice, neutrophils were stained with 5 μg/mL propidium iodide (PI) for 15 min. After washing slightly with PBS thrice, neutrophils were

visualized by ImageXpress Micro system (Molecular Devices, Sunnyvale, CA, USA).

In vivo formation of NETs in control group and LPs-R848-treated group 24 h after injection were analyzed by IF. The slides were stained with Cy3-MPO and DAPI and finally visualized under the slide scanning system (VS200, Olympus, Tokyo, Japan).

2.13. Transportation of MM-LPs-POD from neutrophils to tumor cells

To image the *in vitro* release of nanoparticles from neutrophils to 4T1 cells due to the formation of NETs in the presence of phorbol myristate acetate (PMA), DiD-labeled neutrophils encapsulated with MM-LPs-DiO (neutrophils-DiD/MM-LPs-DiO) were co-cultured with 4T1 cells in medium with 100 nmol/L PMA and observed under ImageXpress Micro system (Molecular Devices). Briefly, 4T1 cells (1×10^4 cells) were seeded in a 96-well plate. After overnight incubation, neutrophil-DiD/MM-LPs-DiO was added to tumor cells and incubated with or without PMA (100 nmol/L) for 8 h. Tumor cells were then washed with PBS slightly to remove suspended neutrophils and uningested nanoparticles followed by staining with DAPI for 30 min to localize cell nuclei.

We also verified this phenomenon *in vivo*. Mice were first i.v. injected or not with LPs-R848 (5 μg of R848 per mouse). One hour later, neutrophils-DiD/MM-LPs-DiO (5×10^6 cells) were i.v. injected. After 20 h, mice were sacrificed, and tumors were digested to analyze DiO signals in transferred neutrophils and tumor cells using flow cytometry (BD). Moreover, tumors, livers and spleens in selected groups were rapidly made into frozen slices for further observation. Upon staining with DAPI to mark cell nuclei, the distribution of fluorescence signals of DiD and DiO was visualized using the slide scanning system (Olympus).

2.14. In vivo antitumor effect in orthotopic breast tumor-bearing mice

The synergistic therapeutic effect of enhanced tumor accumulation of nanoparticles benefitting from neutrophil activation and POD-mediated chemotherapy was studied in the orthotopic 4T1 tumor model. A total of 1×10^6 4T1-luc cells were suspended with matrigel in 100 μL of ice-cold PBS and injected into the right fat pad of mice. When the tumor volume reached approximately 100 mm^3, mice were randomly divided into five groups and received five treatments every other day. The i.v. injection doses of R848 and POD were 5 μg per mouse and 2.5 mg/kg, respectively. For the combination group, the LPs-R848 were i.v. injected 1 h before administration of MM-LPs-POD. The body weight and tumor size were monitored throughout the trial, and the tumor volume was calculated based on the equation as shown in Eq. (1):

$$\text{Tumor volume} = 0.5 \times \text{Length} \times \text{Width}^2 \quad (1)$$

when the tumor size reached approximately 1700 mm^3 in the control group, most of the mice were euthanized and then the tumors and major organs were collected, weighed, photographed and fixed for further studies. The other mice were fed for total 25 days to observe pulmonary metastasis.

2.15. Hematoxylin and eosin (HE) staining and immunohisto chemistry (IHC)

The tumors and main organs were harvested and fixed in 4% paraformaldehyde for 2 days, embedded in paraffin, and sliced for HE staining and immunohistochemistry[35]. To further study the antitumor efficacy of each group, evaluation of tumor cell proliferation and apoptosis was performed by Ki67 and terminal deoxynucleotidyl transferase-mediated dUTP nick end-labeling (TUNEL) staining according to the manufacturer's instructions. For the immunohistochemical staining of Ly6G, tumors from mice untreated and treated with LPs-R848 for 4 h were fixed and stained with anti-Ly6G antibody. All the slides were observed using the slide scanning system (Olympus).

2.16. Statistical analysis

Data are expressed as the mean±SD of at least three independent experiments. All statistical analyses were conducted in GraphPad Prism 8.0 (GraphPad Software, San Diego, CA, USA) using an unpaired two-tailed Student's *t*-test. When the P value < 0.05 or less, data from two groups were considered statistically significant.

3. Results and discussion

3.1. Preparation and characterization of MM-LPs-POD

MM-LPs-POD were prepared through the top-down method with the committed step of coextrusion. LPs-POD were first obtained by the conventional thin-film hydration method (Fig. 1A). MM was isolated using repeated freeze−thaw cycles under hypotonic conditions followed by two-step centrifugation. The protein quantification of purified MM was performed using a BCA assay, and the average protein content of the membrane extracted from 500 mL culture medium was estimated to be ~2 mg. The membrane was stored at −80 °C in lyophilized form until use. HPLC analysis indicated that the encapsulation efficiency of POD was 91.26%. To investigate the optimal mass ratio of LPs to MM, an *in vivo* imaging experiment was carried out. Hybrid LPs at various ratios of LPs to MM were prepared and labeled with DiD followed by i.v. injection into mice, and photos were taken at different time points (Fig. 1B). We found that nanoparticles accumulated in tumors over time in all groups, among which the 2:0.04 group exhibited the strongest tumor-targeting capacity. The results were further confirmed by *ex vivo* fluorescence imaging (Fig. 1C) and relative ROI analysis quantification (Fig. 1D and E). These results indicated that the ratio of 2:0.04 was the optimal one for MM-LPs to hijack neutrophils effectively *in vivo* and realize tumor targeted accumulation. Therefore, the ratio of 2:0.04 was employed in the preparation of MM-LPs in further studies. The assembly of MM fuses with the lipid components of the LPs driven by mechanical force from ultrasound and agitation and hence forms stable MM-LPs. To confirm the fusion of the isolated MM and the synthetic LPs, an FRET study was conducted by fusing FRET dye (DiD and DiI)-labeled LPs with increasing amounts of MM. There was a fluorescence recovery at 567 nm (DiI) and a fluorescence decrease at 664 nm (DiD) with an increasing weight ratio of MM to LPs (Fig. 1J), indicating successful fusion between the two membrane materials and a weakened FRET effect of the dyes. Then, the protein profiles of MMVs and MM-LPs were determined by SDS-

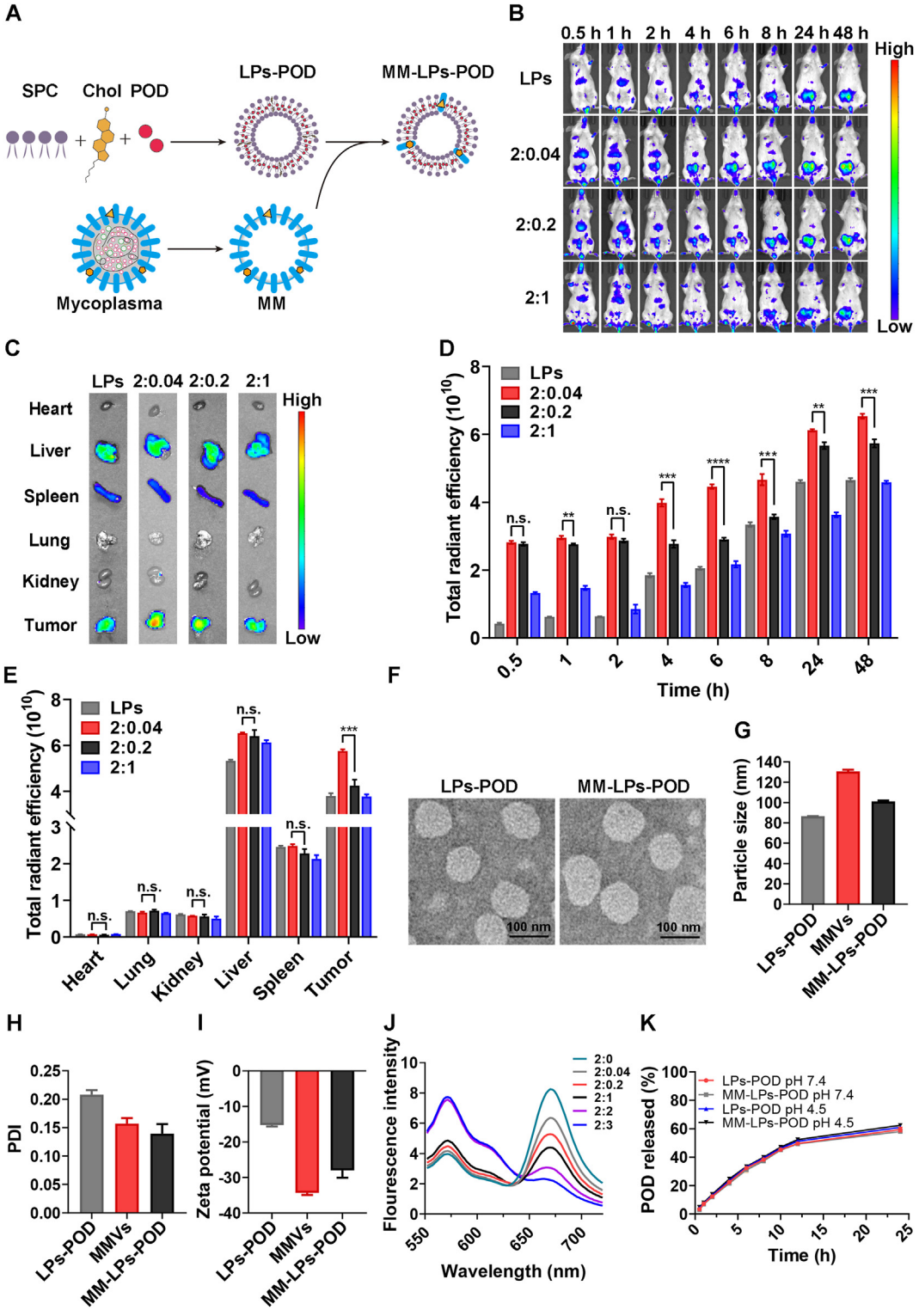

Figure 1 Fabrication and *in vitro* characterization of MM-LPs-POD. (A) Schematic illustration of the preparation of MM-LPs-POD (B−E) Optimization of the mass ratio of LPs to MM protein was studied by IVIS. (B) Representative living images and (C) *ex vivo* fluorescence imaging of tumors and main organs excised from mice at 48 h after injection. (D) Corresponding quantitative analysis of fluorescence intensity at the tumor sites ($n=3$). (E) Corresponding quantitative analysis of fluorescence intensity of major organs ($n=3$). (F) TEM imaging (G) size, (H) PDI, and (I) zeta potential of LPs-POD and MM-LPs-POD ($n=3$). (J) LPs stained with FRET pair-dyes DiD and DiI were fused with increasing ratios of MM and fluorescence spectrum was recorded. The ratio represents the mass ratio of LPs to MM protein (K) *In vitro* cumulative drug release of LPs-POD and MM-LPs-POD in PBS at pH values of 7.4 and 4.5. Data are shown as the mean±SD and analyzed by unpaired two-tailed Student's *t*-test. *$P<0.05$, **$P<0.01$, ***$P<0.001$. n.s., not significant.

PAGE assay. Compared with MMVs, MM-LPs retained almost all of the cell membrane proteins (Supporting Information Fig. S1A). Additionally, the western blotting result revealed that typical membrane protein of mycoplasma cells (P97) was present on MM-LPs without loss during the fusion process (Fig. S1B).

Furthermore, the morphology and hydrodynamic nature of each nanoparticle were characterized by TEM (HITACHI) and DLS (Malvern Panalytical). MM-LPs-POD presented as spherical vesicular structure, which was similar to that of conventional liposomes (LPs-POD, Fig. 1F). MMVs showed a typical double-layer membrane structure (Supporting Information Fig. S2). As measured by DLS, the average size of MM-LPs-POD was 101.4 nm with the narrowest size distribution, while MMVs were relatively larger (Fig. 1G and H, and Supporting Information Fig. S3), which was possibly due to the mechanical rigidity of the pure MM. Moreover, the zeta potential value of MM-LPs-POD was between that of MMVs and LPs-POD (Fig. 1I), which further verified the valid fusion of MM with LPs. The stability of LPs-POD and MM-LPs-POD was further investigated by monitoring the size change of diluents in saline and 10% FBS at 4 and 37 °C. Both preparations remained stable during the trial (Supporting Information Figs. S4 and S5). Finally, the drug-releasing profiles showed no significant differences between the two nanoparticles under all experimental conditions (Fig. 1K).

3.2. *LPs-R848 notably enhanced neoplastic infiltration of neutrophils*

R848, which serves as a TLR7/8 agonist, could induce a pronounced immune response and has been extensively studied for the treatment of a variety of tumors in nanoparticle form and other forms[23,25,28]. It was reported that R848 could activate neutrophils in the blood and significantly increase neutrophil frequency in tumors. To investigate the effect of R848 on neutrophils and avoid systemic toxicity, we encapsulated R848 into LPs and measured the number of neutrophils in blood and tumors by flow cytometry (BD) at different time intervals after i.v. injection (Fig. 2D). To determine the minimal and effective dose, tumor-bearing mice were primarily i.v. injected with various doses of R848 (1, 5, 10, and 20 μg per mouse) and analyzed after 4 h; typical gating strategies are shown in Supporting Information Fig. S6. The results suggest that administration of LPs-R848 at 5 μg per mouse could dramatically increase the proportion of neutrophils in $CD45^+$ leukocytes in both in the blood and tumor (Fig. 2A and B, and Supporting Information Fig. S7). The 1 μg group failed to increase the neutrophil ratio in the tumor despite elevated levels being observed in the blood. Hence, a dose of 5 μg per mouse was applied in the following experiment. From the perspective of the proportion change of neutrophils over time, a conspicuous increase of $CD45^+CD11b^+Ly6G^+$ neutrophils was observed in the tumors within 8 h post administration of LPs-R848 and peaked at 4 h (Fig. 2G and H). Immunohistochemical staining of Ly6G also confirmed the promoting effect of LPs-R848 on tumor infiltration of neutrophils (Supporting Information Fig. S8). In the blood samples, this elevated status persisted for at least 24 h (Fig. 2E and F), which can be interpreted as the breakdown of neutrophils taking place upon killing tumor cells prior to neutrophil accumulation. In addition to the tumors we expected, the liver and spleen, which act as critical immune tissues and host a wide range of immunologic functions[36,37], are two organs where undesirable nanoparticle accumulation may occur. We next sought to explore the changes in the mRNA levels of the major chemokines responsible for neutrophil recruitment, such as *Cxcl1*, *Cxcl2*, and *Cxcl5*. As evident in Fig. 2C, although slight upregulation of the expression levels of these three genes was observed in the livers upon LPs-R848 treatment, their elevation was most pronounced in inflammatory tumors, as expected. Moreover, almost no obvious change was exhibited in the spleen after LPs-R848 treatment. These results clearly suggested that LPs-R848 had the ability to activate neutrophils in the blood and specifically help recruit neutrophils into tumors, thus creating the prerequisites for the accumulation of more nanoparticles.

3.3. *Concomitant enhanced nanoparticle accumulation in tumors upon neutrophil recruitment induced by LPs-R848*

To demonstrate the indispensable role of circulating neutrophils in the delivery of nanoparticles to the tumor, we conducted an *in vivo* colocalization experiment of neutrophils and nanoparticles and evaluated them by flow cytometry (BD). Tumor-bearing mice were i.v. injected with LPs-R848, followed by injection with LPs-DiD 1 h later. Then, at different time points, the tumor and blood samples were retrieved, and cells were stained for analysis by flow cytometry (BD). The time interval between LPs-R848 and LPs-DiD was determined by the change in the percentage of neutrophils over time in blood after treatment with LPs-R848, and at 1 h post injection, the percentage of neutrophils was significantly upregulated but had not yet peaked. Initially, we found that the percentage of circulating neutrophils containing DiD^+ LPs increased in a time-dependent manner (Fig. 3A and C), which was consistent with the data from tumor tissue (Fig. 3D and Supporting Information Fig. S9A) without treatment with LPs-R848 in advance. Under the activation of LPs-R848, the colocalization of the two unsurprisingly remained time-dependent, and the value was significantly higher (Fig. 3B−D and Fig. S9B). These results demonstrated that R848-activated neutrophil infiltration promotes the accumulation of nanoparticles in tumors.

3.4. *MM-LPs hijacked neutrophils more efficiently, thus achieving more tumor accumulation*

The *in vivo* imaging studies mentioned above illustrated that the tumor-targeting ability of MM-modified nanoparticles was much better than that of simple LPs. To verify whether this advantage is contributed by the increased uptake of MM-LPs by neutrophils and to clarify the role of LPs-R848 in this process, flow cytometry analysis was performed to investigate the ratio of neutrophils carrying nanoparticles post injection with MM-LPs-DiD with or without LPs-R848 pretreatment. As shown in Fig. 3E and F, and Supporting Information Fig. S10, aligning with the results of LPs-DiD, the co-localization of neutrophils and MM-LPs-DiD was strikingly enhanced by LPs-R848 activation. More importantly, MM-LPs could hijack circulating neutrophils more efficiently than simple LPs regardless of the presence of LPs-R848. In addition, an *in vivo* imaging system was used for further study of the targeted delivery of nanoparticles. These results demonstrated that LPs presented a remarkably stronger capability of tumor-targeting after treatment with LPs-R848, which was consistent with the results described above. In addition, in the presence of LPs-R848, MM-LPs still showed better tumor-targeting properties than LPs (Fig. 3G and H, and Supporting Information Fig. S11). Therefore, we can conclude that both pre-injection of LPs-R848 and modification with MM could promote the accumulation of LPs in tumor site. That is, the introduction of MM into LPs significantly enhanced the tumor-targeting ability by hijacking circulating neutrophils in a rapid and powerful manner when assisted by LPs-R848.

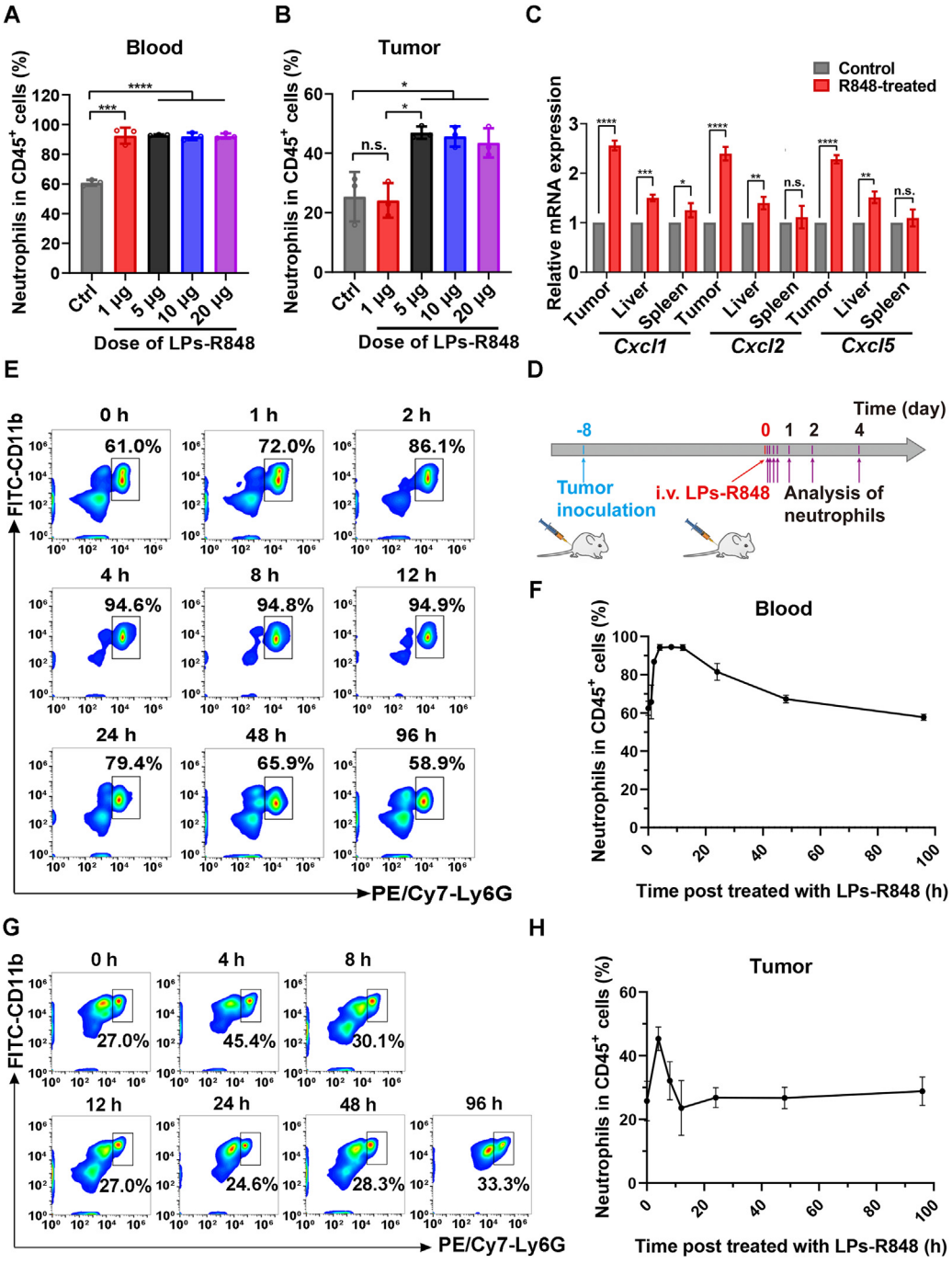

Figure 2 LPs-R848 activated neoplastic infiltration of neutrophils. Effects of different doses of R848 on neutrophil percentages among total $CD45^+$ leukocytes in (A) blood and (B) tumors ($n=3$). (C) Relative mRNA levels of three chemokines, *Cxcl1*, *Cxcl2* and *Cxcl5*, in tumors, liver and spleen with or without LPs-R848 pretreatment ($n=3$). (D) Schematic diagram of the analysis of the change in neutrophil proportion among total $CD45^+$ leukocytes post injection of R848. Eight days after tumor inoculation, LPs-R848 were i.v. injected into mice (5 μg per mouse). At different time intervals, the tumors and blood were harvested for experiments. (E) Flow cytometry graphs and (F) corresponding quantitative analysis of neutrophil proportion in total $CD45^+$ leukocytes post injection of R848 at the indicated time points in blood samples ($n=5$). (G) and (H) show data from tumor tissue samples ($n=5$). Data are shown as the mean±SD and analyzed by unpaired two-tailed Student's *t*-test. $^*P<0.05$, $^{**}P<0.01$, $^{***}P<0.001$, $^{****}P<0.0001$. n.s., not significant.

3.5. *MM-LPs-POD showed no toxicity to neutrophils*

To evaluate the toxicity of MM-LPs-POD to neutrophils *in vitro*, we first characterized the physiological functions of the extracted neutrophils. Mature neutrophils were isolated from the bone marrow of mice through the commonly used density gradient centrifugation method. The average yield of neutrophils was approximately 6×10^6 cells per mouse, and the viability was 98% as calculated by trypan blue exclusion on a slide. Dual staining with FITC-CD11b and PE/Cy7-Ly6G antibodies indicated that the purity was above 94% (Fig. 4A). CD11b and CD44 are specific proteins on the surface of neutrophils, which are related to the adhesion and migration of

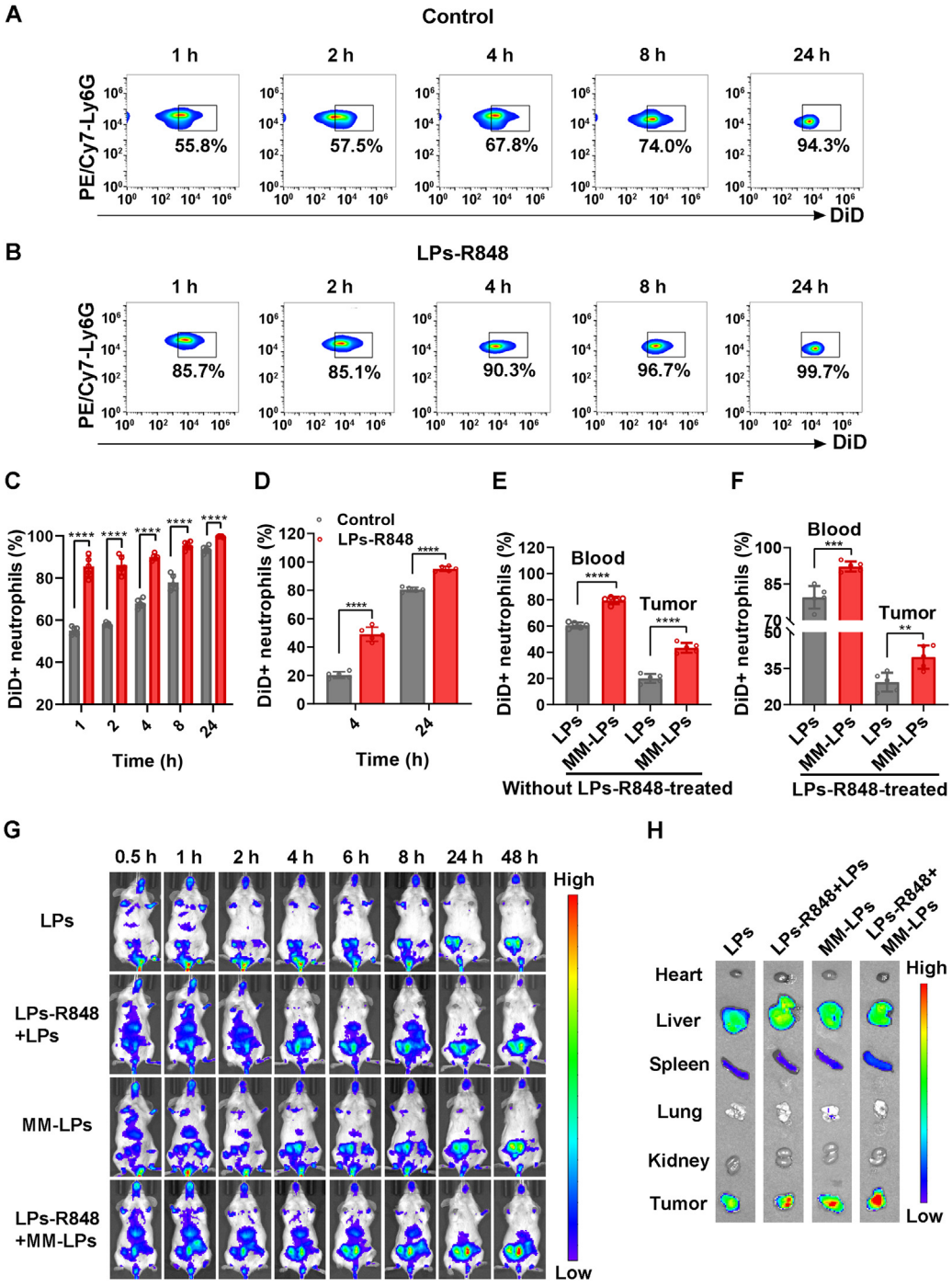

Figure 3 Both treatment with LPs-R848 and modification of LPs with MM could enhance the *in vivo* ingestion of nanoparticles by neutrophils, which in turn facilitated nanoparticle accumulation at tumor sites. (A−F) LPs-DiD and MM-LPs-DiD were i.v. injected into tumor-bearing mice with or without LPs-R848 pretreatment. At different time intervals post nanoparticle injection, the tumors and blood were harvested to analyze the DiD^+ neutrophil percentage using flow cytometry. After injection of LPs-DiD, the change in DiD^+ neutrophil percentage in the blood of (A) the control group or (B) LPs-R848-pretreated group was determined ($n=5$). Corresponding histograms of (C) the blood sample and (D) tumor tissue ($n=5$). (E) Quantitative figure comparing the DiD^+ neutrophil percentage between the LPs-DiD group and MM-LPs-DiD group at 4 h after injection without LPs-R848 pretreatment ($n=5$). (F) Quantitative figure comparing the DiD^+ neutrophil percentage between the LPs-DiD group and the MM-LPs-DiD group at 1 h after injection with LPs-R848 pretreatment ($n=5$). (G) *In vivo* imaging of mice and (H) *ex vivo* imaging of organs at different time points after injection of LPs-DiD or MM-LPs-DiD with or without LPs-R848 pretreatment ($n = 3$). Data are shown as the mean±SD and analyzed by unpaired two-tailed Student's t-test. *$P<0.05$, **$P<0.01$, ***$P<0.001$, ****$P<0.0001$. n.s., not significant.

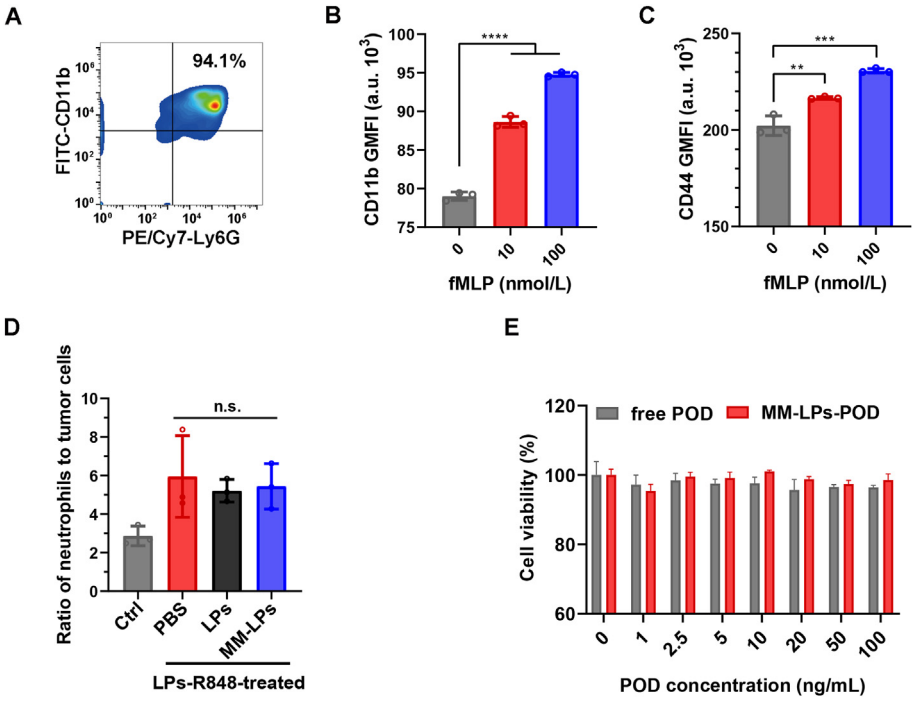

Figure 4 Evaluation of physiological activities of neutrophils. (A) Flow cytometry analysis of the purity of isolated neutrophils that were double-stained with FITC-CD11b and PE/Cy7-Ly6G antibodies. Expression of (B) CD11b and (C) CD44 on the surface of neutrophils isolated from mice after treatment with different concentrations of fMLP for 0.5 h ($n=3$). CD11b and CD44 were stained with FITC-CD11b and APC-CD44 antibodies respectively. (D) Study of the ratios of neutrophils to tumor cells before and after administration of nanoparticles. Mice were pretreated with or without LPs-R848 and injected with PBS, LPs and MM-LPs 1 h later. The ratios of neutrophils to tumor cells were analyzed using flow cytometry ($n=3$). (E) Cytotoxicity of free POD and MM-LPs-POD against neutrophils for 12 h ($n=3$). Data are shown as the mean±SD and analyzed by unpaired two-tailed Student's *t*-test. $^{**}P<0.01$, $^{***}P<0.001$, $^{****}P<0.0001$. n.s., not significant.

neutrophils and could be upregulated under the stimulation of inflammation[38,39], therefore acting as signs of whether neutrophils maintain normal physiological functions. fMLP is a neutrophil chemotactic peptide which is often used to mimic the chemotactic process[40]. We used flow cytometry (BD) to estimate CD11b and CD44 expression on the isolated neutrophil surfaces after stimulation with fMLP. Fig. 4B and C, and Supporting Information Fig. S12 suggested that the expression of the two proteins was significantly increased following treatment with fMLP. To identify whether the uptake of nanoparticles altered the ability of neutrophils to infiltrate into tumors, tumor-bearing mice pretreated with LPs-R848 were i.v. injected with PBS, LPs and MM-LPs respectively, and 4 h later, the ratio of neutrophils to tumor cells was calculated based on flow cytometry analysis. In addition to the enhanced neutrophils infiltration benefited from LPs-R848 corresponding to the conclusion mentioned above (Fig. 4D). The ratios of the three injection groups exhibited no significant difference. Taken together, these results illustrated that the neutrophils we isolated maintained their normal physiological function and that the uptake of nanoparticles did not affect the tumor infiltration ability of the neutrophils.

The cytotoxicity of free POD and MM-LPs-POD towards neutrophils *in vitro* was examined using the CCK-8 assay at POD concentrations from 0 to 100 ng/mL. As illustrated in Fig. 4E, unlike other chemotherapeutics[12,17], even high doses of POD did not cause any toxicity to neutrophils. Likewise, MM-LPs-POD were also nontoxic to neutrophils at the concentrations used. This outcome provided a foundation for the use of neutrophils as vehicles for the delivery of MM-LPs-POD.

3.6. Intercellular transport of loaded MM-LPs from neutrophils to tumor cells under inflammation

The release of nanoparticles from cell carriers and uptake by targeted tissues warrants attention when designing drug delivery systems[7]. Neutrophils are superior vectors because inflammatory signals in the tumor microenvironment can induce the apoptosis of neutrophils and form NETs, followed by the release of loaded contents[12,41]. We used PMA to simulate an inflammatory environment[42]. First, we observed that neutrophils formed NETs successfully under the stimulation of PMA, which was manifested by the disintegration of plasma membrane (Supporting Information Fig. S13). Neutrophils-DiD/MM-LPs-DiO were first fabricated (Supporting Information Fig. S14) and cocultured with tumor cells with or without 100 nmol/L PMA for 8 h (Fig. 5A). The release and reuptake of nanoparticles was visualized by fluorescence imaging. More nanoparticles colocalized with tumor cells in the PMA-treated group, whereas nanoparticles mostly remained in neutrophils in the absence of PMA (Fig. 5B). Quantitative calculation demonstrated that about 86% of the POD released from neutrophils was encapsulated in MM-LPs. Furthermore, the integrity of released MM-LPs-POD was confirmed by TEM (Supporting Information Fig. S15). These data suggested that in response to inflammation induction, neutrophils could form NETs and release MM-LPs-POD, which could maintain stability and structural integrity.

To achieve a comprehensive evaluation, we also carried out the corresponding experiment *in vivo*. We first verified the formation of NETs in tumors treated with LPs-R848 for 24 h by co-staining with

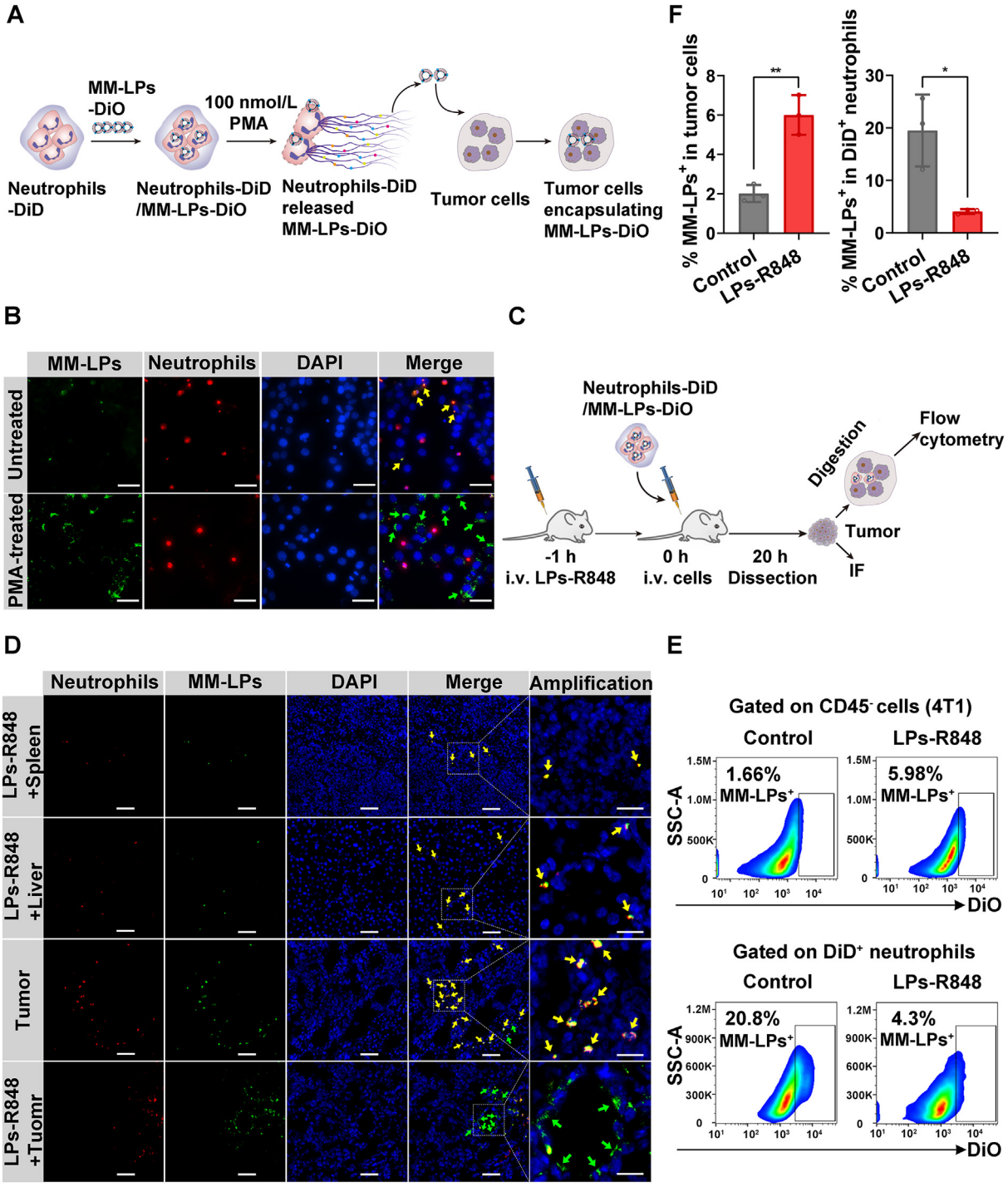

Figure 5 Transportation of nanoparticles from neutrophils to tumor cells under inflammation. (A) Schematic pattern of neutrophils and the 4T1 coculture model. DiD-labeled neutrophils were incubated with MM-LPs-DiO for 1 h, and then the resulting neutrophils-DiD/MM-LPs-DiO were incubated with tumor cells with PMA for 8 h followed by DAPI staining and microscope observation. (B) Imaging of the coculture model. Yellow and green arrows represent MM-LPs-DiO colocalized with neutrophil-DiD and tumor cells, respectively. Scale bar: 20 μm. Data are representative of three biological replicates. (C) Schematic illustration of 4T1 cells ingesting MM-LPs-DiO released from neutrophils in tumors from mice with or without LPs-R848 treatment. Tumors were collected for IF and flow cytometry experiments. (D) MM-LPs-DiO released from neutrophils and subsequently internalized by the spleen, liver and tumor cells was studied by IF of tissue slices. Yellow and green arrows represent MM-LPs-DiO colocalized with neutrophil-DiD and tumor cells, respectively. The scale bars are 20 μm for the amplification panels and 50 μm for all other panels. Data are representative of three biological replicates. (E) Flow cytometry analysis and (F) corresponding quantitative analysis of the percentage of DiO^+ cells in transferred DiD^+ neutrophils and $CD45^-$ tumor cells (4T1) ($n=3$). Data are shown as the mean±SD and analyzed by unpaired two-tailed Student's *t*-test. $^*P<0.05$, $^{**}P<0.01$.

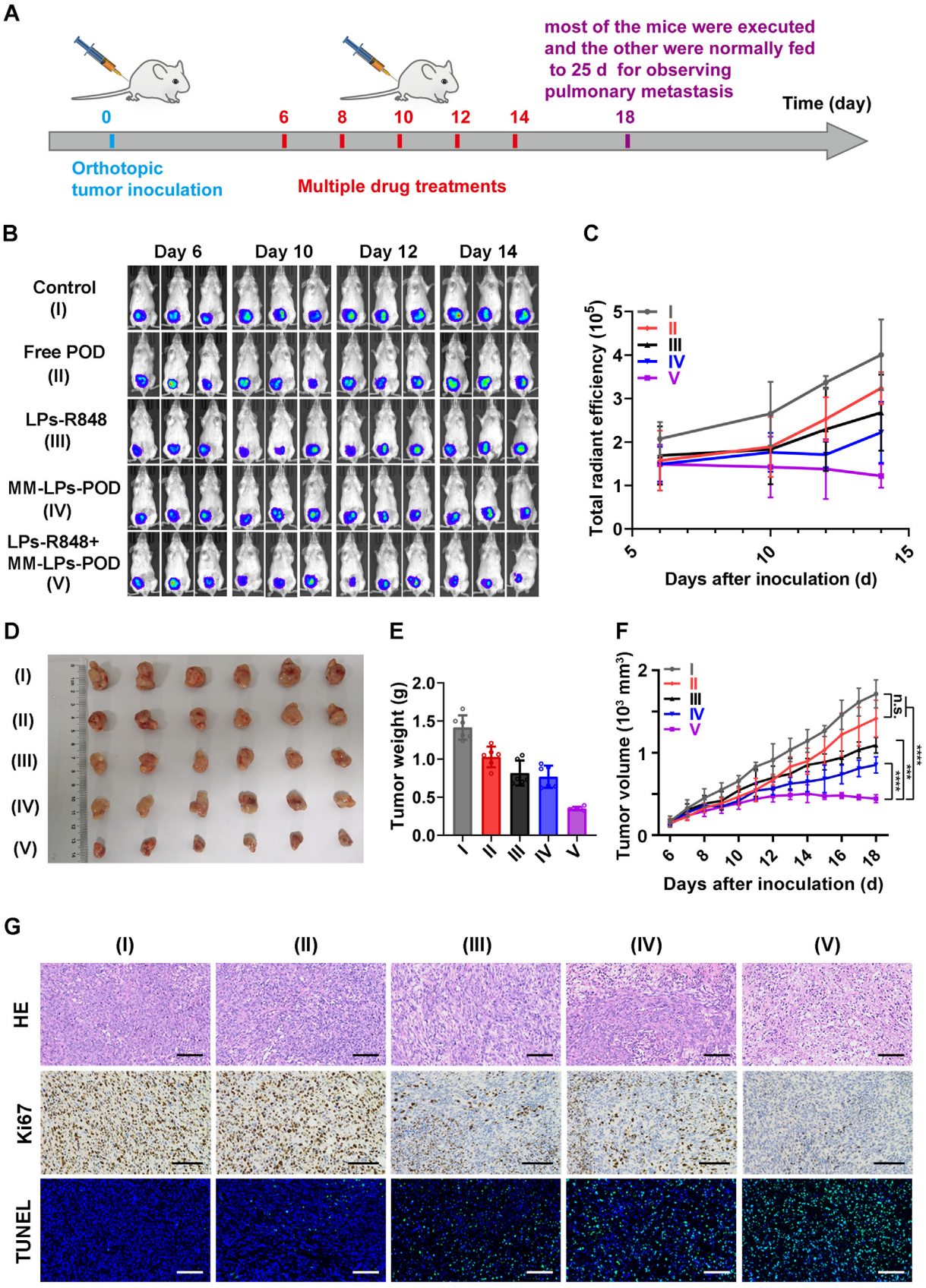

Figure 6 The combination of LPs-R848 with MM-LPs-POD exerted improved antitumor efficacy. (A) Schematic showing of the arrangements for animal experiments. (B) *In vivo* bioluminescence images to monitor the size of tumors in the different groups of mice that received various treatments and (C) the corresponding ROI analysis of tumors. (D) Photos and (E) weight of tumors at the end of the experiment, and (F) change in tumor growth ($n = 6$). (G) Images of HE, Ki67 and TUNEL staining of tumor slices. Scale bar: 100 μm. Data are shown as the mean±SD and analyzed by unpaired two-tailed Student's *t*-test. ***$P<0.001$, ****$P<0.0001$. n.s., not significant.

DAPI and myeloperoxidase (MPO) antibody. The co-localization of DAPI and MPO confirmed the existence of NETs[43−45] (Supporting Information Fig. S16). Next, neutrophils-DiD/MM-LPs-DiO were i.v. injected into tumor-bearing mice pretreated with LPs-R848. After 20 h, tumors, livers and spleens were harvested for further analysis (Fig. 5C). The flow cytometry results in tumors revealed that the percentage of $CD45^-$ tumor cells containing DiO^+ nanoparticles increased at least threefold in the LPs-R848 pretreatment group compared with the control group. Moreover, the percentage of DiD^+ neutrophils carrying DiO^+ nanoparticles dramatically decreased post LPs-R848 treatment (Fig. 5E and F). The results were further confirmed by IF analysis of tumor tissue sections from which the enhanced co-localization of nanoparticles with tumor cells rather than neutrophils in the LPs-R848-treated group was observed (Fig. 5D). To define the distribution of neutrophils-DiD/MM-LPs-DiO in the liver and spleen, an IF experiment was conducted. As shown in Fig. 5D, the transferred nanoparticles loading neutrophils were much less distributed in the liver and spleen than in tumors. Moreover, the antiproliferation activity of PMA-treated MM-LPs-POD against 4T1 cells was investigated using a CCK-8 assay (Supporting Information Fig. S17). MM-LPs-POD/neutrophils stimulated by PMA presented considerable cytotoxicity to MM-LPs-POD, and both of them are stronger than free POD, which suggested that MM-LPs-POD released from neutrophils in response to inflammatory stimulation remained intact and were cytotoxic. Together, these results demonstrated that neutrophils mainly deliver the nanoparticles they carry to the tumor site and then successfully release nanoparticles that are absorbed by tumor cells driven by the inflammatory environment and finally, exert antitumor effects.

3.7. *Pharmacokinetics*

The blood concentration−time profiles and the mean pharmacokinetic parameters of free POD and MM-LPs-POD are shown in Supporting Information Fig. S18. The results indicated that the blood circulation half-life ($t_{1/2}$) of POD in free form (free POD) and loaded in MM-LPs (MM-LPs-POD) was 0.857 and 2.345 h, respectively. Furthermore, MM-LPs-POD increased the total platinum exposure in plasma with an AUC 2.4-fold higher than that of free POD. Taken together, these data suggested that POD loaded in MM-LPs exhibited a superior blood circulation profile compared with the free form.

3.8. *In vivo synergistic antitumor activity and safety evaluation*

The synergistic antitumor effect of R848-mediated neutrophil infiltration combined with POD-mediated chemotherapy was evaluated in the orthotopic 4T1-luc tumor-bearing mouse model (Fig. 6A). For the combination therapy group (referred to as the LPs-R848+MM-LPs-POD group), as in the previous experiment, mice were pretreated with LPs-R848 at a dose of 5 μg per mouse 1 h before injection of MM-LPs-POD (2.5 mg/kg) to induce an acute inflammatory environment. *In vivo* bioluminescence imaging was examined four times on Days 6, 10, 12 and 14 for clearer observation of tumor growth. Moreover, the body weight of the mice and tumor size were monitored during the experiment. At the end of the study, tumors were harvested and weighed to verify the antitumor effects of each group.

The results of bioluminescence imaging indicated comparable tumor sizes on Day 6, and as the treatment progressed, the tumors in the control group developed rapidly while the combination group ended up with only a small area of fluorescence, indicating that tumors were severely suppressed (Fig. 6B). The outcomes were further confirmed by ROI analysis (Fig. 6C). As presented in Fig. 6D−F, the free POD group had a slight tumor-destroying effect but did not display a significant difference from the control group. Both LPs-R848 and MM-LPs-POD destroyed tumors only moderately. While the combination group showed the strongest inhibition of tumor growth and pulmonary metastasis expectedly even at the pretty low dose of POD (Supporting Information Fig. S19). In addition, most of the apoptosis and severely inhibited proliferation were found in the combination group through HE, Ki67 and TUNEL staining of tumor sections (Fig. 6G). Ultimately, we addressed the safety of treatment regimens through changes in body weight, viscera-related serological indexes and HE staining (Supporting Information Figs. S20−S22). From the results of serum ALT and AST levels, the tumor burden itself caused a great degree of liver damage, leading to the significant upregulation of these two indicators. The lower levels of ALT and AST in LPs-R848+MM-LPs-POD group might benefit from its better oncology efficacy. In general, these findings revealed that none of the treatment groups manifested any systemic toxicity due to the relatively low POD dosage of administration. In summary, LPs-R848-induced immunomodulation and neutrophil recruitment combined with sufficient aggregation of MM-LPs-POD-enhanced antitumor chemotherapy represented a typical synergistic therapy that significantly restrained tumor progression and metastasis in 4T1 breast cancer. More importantly, this combination significantly reduced the effective doses of the two drugs with relatively high toxicity.

4. Conclusions

To sum up, we established an MM-modified LPs drug delivery system that can hijack activated neutrophils and enable tumor homing along with neutrophil recruitment under the stimulation of the immune activator R848. Adding pathogenic characteristics bestowed the nanocarriers with active targeting and accumulation deep within tumors, thus accordingly enhancing the efficacy of the loaded chemotherapeutic drug. This approach resulted in a remarkable improvement in the suppression of tumor growth and metastasis in the 4T1 orthotopic breast tumor model. Therefore, this therapeutic strategy possesses the potential to treat a wide range of cancers through tumor-targeted drug delivery conferred by circulating neutrophils, surmounts the barrier of limited accumulation of nanocarriers in tumors, and represents a promising strategy with clinical feasibility.

Acknowledgments

This work was supported by the National Natural Science Foundation of China (81872986), the "Double First-Class" University project (CPU2018GF03, China), the 111 Project from the Ministry of Education of China, and the State Administration of Foreign Export Affairs of China (B18056), the Drug Innovation Major Project (2018ZX09711-001-007, 2018ZX09735002-003, China).

Author contributions

Lingyi Kong and Chao Zhang initiated and supervised the research. Xiaobei Cheng designed and performed the experiments,

interpreted the data, and drafted the manuscript. Pei Yu established the orthotopic 4T1-luc tumor-bearing mouse model and helped to design and perform the experiments. Xiang Zhou guided the experiments and helped to analyze the experimental results. Jiale Zhu and Yubao Han isolated neutrophils from mouse bone marrow and performed partial cellular assays. All authors read and approved the final manuscript.

Conflicts of interest

The authors have no conflicts of interest to declare.

Appendix A. Supporting information

Supporting data to this article can be found online at https://doi.org/10.1016/j.apsb.2021.08.018.

References

1. Brenner DR, Brockton NT, Kotsopoulos J, Cotterchio M, Boucher BA, Courneya KS, et al. Breast cancer survival among young women: a review of the role of modifiable lifestyle factors. *Cancer Causes Control* 2016;**27**:459−72.
2. Zhou P, Qin JQ, Zhou C, Wan GY, Liu YY, Zhang MM, et al. Multifunctional nanoparticles based on a polymeric copper chelator for combination treatment of metastatic breast cancer. *Biomaterials* 2019;**195**:86−99.
3. Xu C, Yang S, Jiang Z, Zhou J, Yao J. Self-propelled gemini-like LMWH-scaffold nanodrugs for overall tumor microenvironment manipulation *via* macrophage reprogramming and vessel normalization. *Nano Lett* 2020;**20**:372−83.
4. Yong TY, Zhang XQ, Bie NN, Zhang HB, Zhang XT, Li FY, et al. Tumor exosome-based nanoparticles are efficient drug carriers for chemotherapy. *Nat Commun* 2019;**10**:3838.
5. Malhotra S, Dumoga S, Joshi A, Mohanty S, Singh N. Polymeric micelles coated with hybrid nanovesicles enhance the therapeutic potential of the reversible topoisomerase inhibitor camptothecin in a mouse model. *Acta Biomater* 2021;**121**:579−91.
6. Combes F, Meyer E, Sanders NN. Immune cells as tumor drug delivery vehicles. *J Control Release* 2020;**327**:70−87.
7. Chu DF, Dong XY, Shi XT, Zhang CY, Wang ZJ. Neutrophil-based drug delivery Systems. *Adv Mater* 2018;**30**:e1706245.
8. Gershkovitz M, Caspi Y, Fainsod-Levi T, Katz B, Michaeli J, Khawaled S, et al. TRPM2 mediates neutrophil killing of disseminated tumor cells. *Cancer Res* 2018;**78**:2680−90.
9. Beauvillain C, Delneste Y, Scotet M, Peres A, Gascan H, Guermonprez P, et al. Neutrophils efficiently cross-prime naive T cells *in vivo*. *Blood* 2007;**110**:2965−73.
10. Yang M, McKay D, Pollard JW, Lewis CE. Diverse functions of macrophages in different tumor microenvironments. *Cancer Res* 2018;**78**:5492−503.
11. Chu DF, Zhao Q, Yu J, Zhang FY, Zhang H, Wang ZJ. Nanoparticle targeting of neutrophils for improved cancer immunotherapy. *Adv Health Mater* 2016;**5**:1088−93.
12. Xue JW, Zhao ZK, Zhang L, Xue LJ, Shen SY, Wen YJ, et al. Neutrophil-mediated anticancer drug delivery for suppression of postoperative malignant glioma recurrence. *Nat Nanotechnol* 2017;**12**:692−700.
13. Che J, Najer A, Blakney AK, McKay PF, Bellahcene M, Winter CW, et al. Neutrophils enable local and non-invasive liposome delivery to inflamed skeletal muscle and ischemic heart. *Adv Mater* 2020;**32**:e2003598.
14. Lyu JY, Wang LJ, Bai XS, Du XJ, Wei J, Wang JX, et al. Treatment of rheumatoid arthritis by serum albumin nanoparticles coated with mannose to target neutrophils. *ACS Appl Mater Interfaces* 2021;**13**:266−76.
15. Dong XY, Chu DF, Wang ZJ. Leukocyte-mediated delivery of nanotherapeutics in inflammatory and tumor sites. *Theranostics* 2017;**7**:751−63.
16. Chu DF, Dong XY, Zhao Q, Gu JK, Wang ZJ. Photosensitization priming of tumor microenvironments improves delivery of nanotherapeutics *via* neutrophil infiltration. *Adv Mater* 2017;**29**:1701021.
17. Li C, Qiu QJ, Liu M, Liu XR, Hu L, Luo X, et al. Sialic acid-conjugate modified liposomes targeting neutrophils for improved tumour therapy. *Biomater Sci* 2020;**8**:2189−201.
18. Kolaczkowska E, Kubes P. Neutrophil recruitment and function in health and inflammation. *Nat Rev Immunol* 2013;**13**:159−75.
19. Li M, Li SY, Zhou H, Tang XF, Wu Y, Jiang W, et al. Chemotaxis-driven delivery of nano-pathogenoids for complete eradication of tumors post-phototherapy. *Nat Commun* 2020;**11**:1126.
20. Chen Q, Huang GJ, Wu WT, Wang JW, Hu JW, Mao JM, et al. A hybrid eukaryotic-prokaryotic nanoplatform with photothermal modality for enhanced antitumor vaccination. *Adv Mater* 2020;**32**:e1908185.
21. Lou XY, Chen ZC, He ZG, Sun MC, Sun J. Bacteria-mediated synergistic cancer therapy: small microbiome has a big hope. *Nano-Micro Lett* 2021;**13**:1−18.
22. Liu WL, Zou MZ, Liu T, Zeng JY, Li X, Yu WY, et al. Cytomembrane nanovaccines show therapeutic effects by mimicking tumor cells and antigen presenting cells. *Nat Commun* 2019;**10**:3199.
23. Michaelis KA, Norgard MA, Zhu X, Levasseur PR, Sivagnanam S, Liudahl SM, et al. The TLR7/8 agonist R848 remodels tumor and host responses to promote survival in pancreatic cancer. *Nat Commun* 2019;**10**:4682.
24. Cen XH, Liu SW, Cheng K. The role of Toll-like receptor in inflammation and tumor immunity. *Front Pharmacol* 2018;**9**:878.
25. Figueiredo P, Lepland A, Scodeller P, Fontana F, Torrieri G, Tiboni M, et al. Peptide-guided resiquimod-loaded lignin nanoparticles convert tumor-associated macrophages from M2 to M1 phenotype for enhanced chemotherapy. *Acta Biomater* 2020;**S1742**:30561−4.
26. Rodell CB, Arlauckas SP, Cuccarese MF, Garris CS, Li R, Ahmed MS, et al. TLR7/8-agonist-loaded nanoparticles promote the polarization of tumour-associated macrophages to enhance cancer immunotherapy. *Nat Biomed Eng* 2018;**2**:578−88.
27. Chen PM, Pan WY, Wu CY, Yeh CY, Korupalli C, Luo PK, et al. Modulation of tumor microenvironment using a TLR-7/8 agonist-loaded nanoparticle system that exerts low-temperature hyperthermia and immunotherapy for *in situ* cancer vaccination. *Biomaterials* 2020;**230**:119629.
28. Liu YY, Qiao LN, Zhang SP, Wan GY, Chen BW, Zhou P, et al. Dual pH-responsive multifunctional nanoparticles for targeted treatment of breast cancer by combining immunotherapy and chemotherapy. *Acta Biomater* 2018;**66**:310−24.
29. Lu RL, Groer C, Kleindl PA, Moulder KR, Huang A, Hunt JR, et al. Formulation and preclinical evaluation of a Toll-like receptor 7/8 agonist as an anti-tumoral immunomodulator. *J Control Release* 2019;**306**:165−76.
30. Hayashi F, Means TK, Luster AD. Toll-like receptors stimulate human neutrophil function. *Blood* 2003;**102**:2660−9.
31. Janke M, Poth J, Wimmenauer V, Giese T, Coch C, Barchet W, et al. Selective and direct activation of human neutrophils but not eosinophils by Toll-like receptor 8. *J Allergy Clin Immunol* 2009;**123**:1026−33.
32. Imbert TF. Discovery of podophyllotoxins. *Biochimie* 1998;**80**:207−22.
33. Labruere R, Gautier B, Testud M, Seguin J, Lenoir C, Desbene-Finck S, et al. Design, synthesis, and biological evaluation of the first podophyllotoxin analogues as potential vascular-disrupting agents. *ChemMedChem* 2010;**5**:2016−25.
34. Chen YC, Huang MY, Zhang LL, Feng ZL, Jiang XM, Yuan LW, et al. Nagilactone E increases PD-L1 expression through activation of c-Jun in lung cancer cells. *Chin J Nat Med* 2020;**18**:517−25.

35. Li XY, Tao H, Jin C, Du ZY, Liao WF, Tang QJ, et al. Cordycepin inhibits pancreatic cancer cell growth *in vitro* and *in vivo via* targeting FGFR2 and blocking ERK signaling. *Chin J Nat Med* 2020;**18**:345−55.
36. Lewis SM, Williams A, Eisenbarth SC. Structure and function of the immune system in the spleen. *Sci Immunol* 2019;**4**:eaau6085.
37. Shuai ZW, Leung MWY, He XS, Zhang WC, Yang GX, Leung PSC, et al. Adaptive immunity in the liver. *Cell Mol Immunol* 2016;**13**:354−68.
38. Diamond MS, Springer TA. A subpopulation of Mac-1 (CD11b/CD18) molecules mediates neutrophil adhesion to ICAM-1 and fibrinogen. *J Cell Biol* 1993;**120**:545−56.
39. Rouschop KMA, Roelofs J, Claessen N, Martins PD, Zwaginga JJ, Pals ST, et al. Protection against renal ischemia reperfusion injury by CD44 disruption. *J Am Soc Nephrol* 2005;**16**:2034−43.
40. Marasco WA, Phan SH, Krutzsch H, Showell HJ, Feltner DE, Nairn R, et al. Purification and identification of formyl-methionyl-leucyl-phenylalanine as the major peptide neutrophil chemotactic factor produced by Escherichia coli. *J Biol Chem* 1984;**259**:5430−9.
41. Papayannopoulos V. Neutrophil extracellular traps in immunity and disease. *Nat Rev Immunol* 2018;**18**:134−47.
42. Brinkmann V, Reichard U, Goosmann C, Fauler B, Uhlemann Y, Weiss DS, et al. Neutrophil extracellular traps kill bacteria. *Science* 2004;**303**:1532−5.
43. Tan C, Aziz M, Wang P. The vitals of NETs. *J Leukoc Biol* 2021;**110**:797−808.
44. de Buhr N, von Köckritz-Blickwede M. How neutrophil extracellular traps become visible. *J Immunol Res* 2016;**2016**:4604713.
45. Nakazawa D, Tomaru U, Yamamoto C, Jodo S, Ishizu A. Abundant neutrophil extracellular traps in thrombus of patient with microscopic polyangiitis. *Front Immunol* 2012;**3**:333.